





Lithium diffusion in LiMnPO_4 detected with $\mu^\pm\text{SR}$

Jun Sugiyama ^{1,2,3,*}, Ola Kenji Forslund ⁴, Elisabetta Nocerino,⁴ Nami Matsubara,⁴ Konstantinos Papadopoulos ⁵, Yasmine Sassa,⁵ Stephen P. Cottrell,⁶ Adrian D. Hillier,⁶ Katsuhiko Ishida,⁷ Martin Månsson,⁴ and Jess H. Brewer ^{8,9}

¹Neutron Science and Technology Center, Comprehensive Research Organization for Science and Society (CROSS), Tokai, Ibaraki 319-1106, Japan

²Advanced Science Research Center, Japan Atomic Energy Agency, Tokai, Ibaraki 319-1195, Japan

³High Energy Accelerator Research Organization (KEK), Tokai, Ibaraki 319-1106, Japan

⁴Department of Applied Physics, KTH Royal Institute of Technology, Roslagstullsbacken 21, SE-106 91 Stockholm, Sweden

⁵Department of Physics, Chalmers University of Technology, SE-412 96 Göteborg, Sweden

⁶ISIS Pulsed Neutron and Muon Facility, STFC Rutherford Appleton Laboratory, Harwell Oxford, Didcot OX11 0QX, United Kingdom

⁷Meson Science Laboratory, RIKEN, 2-1 Hirosawa, Wako, Saitama 351-0198, Japan

⁸Department of Physics and Astronomy, University of British Columbia, Vancouver, British Columbia, V6T 1Z1 Canada

⁹TRIUMF, 4004 Wesbrook Mall, Vancouver, British Columbia, V6T 2A3 Canada



(Received 1 May 2020; revised 29 June 2020; accepted 14 July 2020; published 29 July 2020)

Positive- and negative-muon spin rotation and relaxation ($\mu^\pm\text{SR}$) was first used to investigate fluctuations of nuclear magnetic fields in an olivine-type battery material, LiMnPO_4 , in order to clarify the diffusive species, namely, to distinguish between a μ^+ hopping among interstitial sites and Li^+ ions diffusing in the LiMnPO_4 lattice. Muon diffusion can only occur in $\mu^+\text{SR}$, because the implanted μ^- forms a stable muonic atom at the lattice site, and therefore any change in linewidth measured with $\mu^-\text{SR}$ must be due to Li^+ diffusion. Since the two measurements exhibit a similar increase in the field fluctuation rate with temperature above 100 K, it is confirmed that Li^+ ions are in fact diffusing. The diffusion coefficient of Li^+ at 300 K and its activation energy were estimated to be $1.4(3) \times 10^{-10} \text{ cm}^2/\text{s}$ and 0.19(3) eV, respectively. Such combined $\mu^\pm\text{SR}$ measurements are thus shown to be a suitable tool for detecting ion diffusion in solid-state energy materials.

DOI: [10.1103/PhysRevResearch.2.033161](https://doi.org/10.1103/PhysRevResearch.2.033161)

I. INTRODUCTION

The diffusion coefficient of Li^+ (D_{Li}) is one of the key parameters to determine the charge and discharge rate of any Li-ion battery. While D_{Li} is usually determined with lithium nuclear magnetic resonance (Li-NMR) [1], such determination is extremely difficult for materials that contain magnetic ions [1,2] because of the contribution of electron spins to the spin-lattice relaxation rate ($1/T_1$). Electrochemical measurements also face difficulty in estimating D_{Li} due to the absence of information on the real surface area of materials in a liquid electrolyte [3,4]. It should be noted that ion diffusion plays a significant role not only in battery materials but also in other energy materials [5,6].

We therefore started a project to measure D_{Li} with positive muon spin rotation and relaxation ($\mu^+\text{SR}$) through the observation of fluctuations in the local magnetic fields due to the magnetic moments of Li nuclei diffusing in the lattice [7]. Here, the presence of the μ^+ state in solids indicates that the positive charge of the implanted μ^+ is covered by an electron screening cloud [8,9]. Therefore, $\mu^+\text{SR}$ is expected

to detect the intrinsic change in local magnetic environments induced by Li diffusion. In fact, according to the first attempt on Li_xCoO_2 with $x = 0.53$ and 0.73 (the most common cathode material in the present Li-ion batteries), values of D_{Li} estimated with $\mu^+\text{SR}$ [7] were comparable to those predicted by first principles calculations [10]. Since then, many battery materials have been studied with $\mu^+\text{SR}$ in order to extract their intrinsic D_{Li} [4,11–22] and D_{Na} [23–26].

However, it is well known that while the implanted μ^+ is static at its interstitial site at low temperatures, it starts to diffuse in any solid above a certain temperature [9]. This leads to an ambiguity of the D_{Li} estimated with $\mu^+\text{SR}$ at high temperatures: Are the dynamics really due to Li^+ diffusion alone, or does μ^+ hopping also contribute? This requires confirmation with other techniques. Recently, $\mu^-\text{SR}$ (the negative muon counterpart of $\mu^+\text{SR}$) has been reborn [27] at pulsed muon facilities (J-PARC and ISIS) as a complementary technique for $\mu^+\text{SR}$. Particularly due to the developments of both the μ^- beam and the multidetector counting system [28], $\mu^-\text{SR}$ is now available for detecting internal nuclear magnetic fields in solids [27].

Here, the implanted spin polarized μ^- is captured by a nucleus, resulting in the formation of a muonic atom [29]. Such muonic atoms are stable even at high temperatures or above a chemical decomposition temperature. Unfortunately, the initial μ^- spin polarization is reduced down to about 1/6 during the cascade of the μ^- from the outermost shell orbital to the ground state of a muonic atom, whereas the μ^+ stops almost 100% spin polarized at the interstitial site in the

*juns@triumf.ca; j_sugiyama@cross.or.jp

Published by the American Physical Society under the terms of the Creative Commons Attribution 4.0 International license. Further distribution of this work must maintain attribution to the author(s) and the published article's title, journal citation, and DOI.

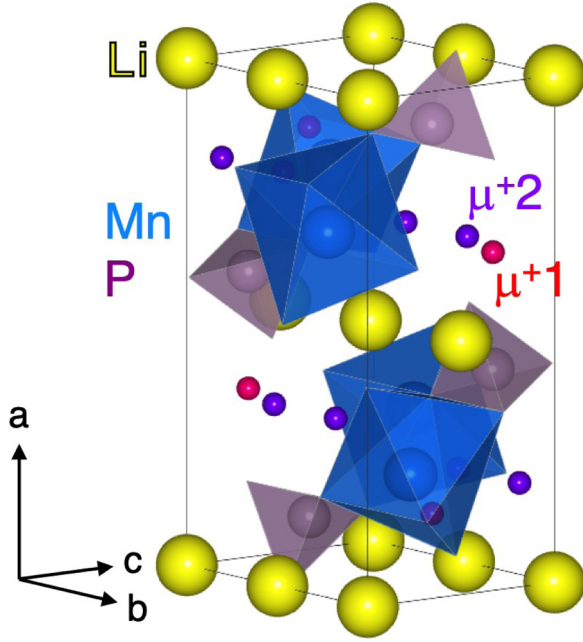


FIG. 1. The crystal structure of LiMnPO_4 in orthorhombic symmetry with space group $Pnma$ drawn by VESTA [30]. Large yellow spheres show Li, medium blue spheres in octahedra show Mn, and medium purple spheres in tetrahedra show P, and small red and magenta spheres represent the two μ^+ sites, μ^+1 (0.135, 0.75, 0.587) and μ^+2 (0.195, 0.92, 0.89) predicted by density functional theory (DFT) calculations with VASP. The corners of each polyhedron are occupied by O (not shown).

lattice. As a result, μ^- SR measurements require very high statistics—at least 36 times higher than for μ^+ SR—to obtain comparably reliable data. This naturally leads to a combined experiment using both μ^+ SR and μ^- SR for detecting D_{Li} . Namely, the diffusing species is determined with μ^- SR, while the detailed temperature dependence of the diffusion is measured with μ^+ SR.

As a first target material for such μ^\pm SR measurements, we have selected an olivine-type lithium manganese phosphate, LiMnPO_4 (see Fig. 1) [31–34], which is heavily investigated as a cathode material for the future Li-ion battery due to its higher working voltage than that for LiFePO_4 . Previous μ^+ SR results reveal that the field fluctuation rate (ν) starts to increase with temperature above ≈ 200 K in LiMPO_4 ($M = \text{Fe}, \text{Co},$ and Ni) regardless of M [12,13,20]. This is probably caused by structural similarities among these compounds, i.e., a one-dimensional diffusion channel along the b axis in LiMPO_4 [35]. However, the question that arises is whether the μ^+ itself is immobile at temperatures above 200 K in the LiMPO_4 lattice, although the μ^+ has been shown to be stable, due to the O- μ^+ bonding in most oxides [8,36,37].

II. EXPERIMENTAL

A powder sample of LiMnPO_4 was purchased from Toshima Manufacturing, Ltd. The μ^- SR time spectra were measured on the decay muon beam line ARGUS at ISIS of Rutherford Appleton Laboratory in the United Kingdom. An approximately 64-g powder sample was placed in a copper

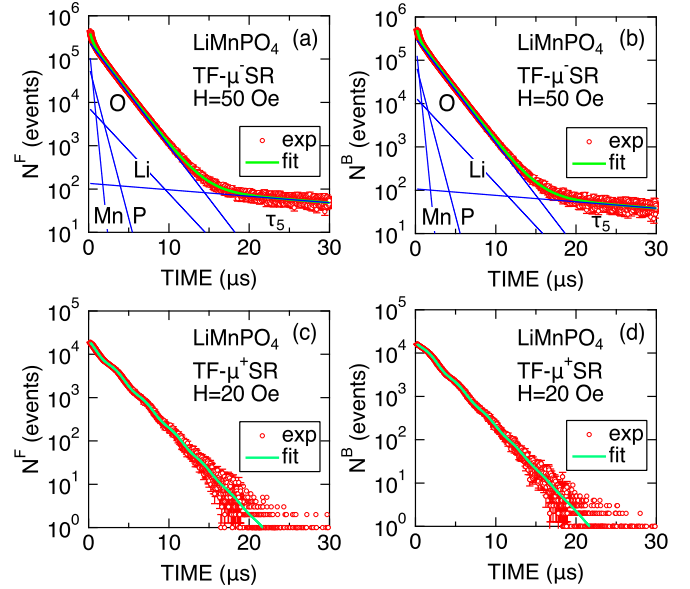


FIG. 2. The time histogram of the TF- μ^- SR spectrum in LiMnPO_4 for the (a) forward counter and (b) backward counter, and that of the TF- μ^+ SR spectrum for the (c) forward counter and (d) backward counter. Red open circles represent the experimental data, green solid lines represent the fit result using Eq. (1), and blue solid lines represent the histograms of the five μ^- lifetimes. In panels (c) and (d), there is naturally only one lifetime component, that of the μ^+ .

container with $4 \times 5 \times 2$ cm³ volume, made of 0.5-mm-thick Cu plate. Two additional Cu plates, each 0.5 mm thick, were attached to the container as a degrader. The copper container was then set onto the bottom of the stick for the He-flow cryostat. The momentum of the μ^- beam was adjusted to 68 MeV/c to maximize the number of μ^- stopped in the sample. The μ^- SR spectrum was measured at 100, 200, and 300 K with up to 50 M events for transverse field (TF) μ^- SR and 250 M events for zero field (ZF) and longitudinal field (LF) μ^- SR at a counting rate of 25 M events/hr. Here, TF [LF] means the applied magnetic field was perpendicular [parallel] to the initial μ^- spin polarization.

The μ^+ SR time spectra were measured on the surface muon beam line EMU at ISIS. An approximately 2-g powder sample from the same batch as for the μ^- SR measurements was packed into an Au O-ring sealed titanium cell. The window of the cell was made of a titanium foil with 20 μm thickness. The cell was then mounted onto the Al plate of a closed-cycle refrigerator-type cryofurnace in the temperature range between 50 and 500 K. The counting rate was about 100 M events/hr. The experimental techniques are described in more detail elsewhere [8,9]. The obtained μ^\pm SR data was analyzed with MUSRFIT [38].

III. RESULTS

A. Histogram for μ^\pm SR

Figure 2 shows the time histograms of the forward and backward counters [$N^F(t)$ and $N^B(t)$] recorded in a TF with $H = 50$ Oe for μ^- SR and $H = 20$ Oe for μ^+ SR. Here, forward (backward) means upstream (downstream) of the sample

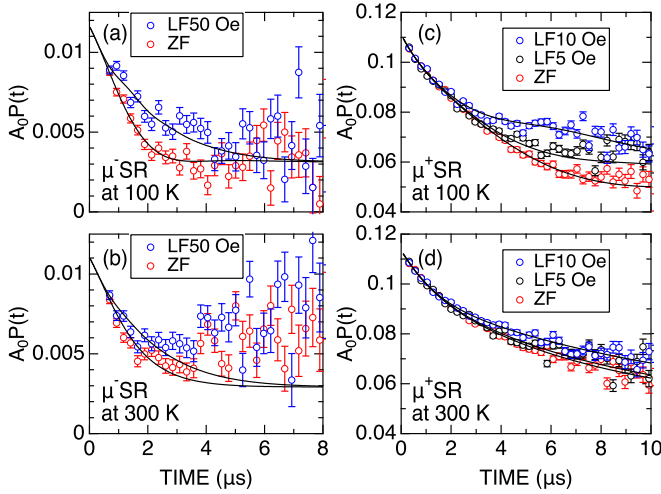


FIG. 3. The ZF- and LF- μ^\pm SR asymmetry spectra for LiMnPO₄; μ^- SR recorded at (a) 100 K and (b) 300 K and μ^+ SR recorded at (c) 100 K and (d) 300 K. The difference of the nonlinear background signal between panels (a) and (b) may be caused by the change in dynamics of μ^- -Li with temperature. In panels (a) and (b), solid lines represent the best fit in the time domain between 0.5 and 3 μ s using Eq. (4), whereas in panels (c) and (d) they represent the best fit in the time domain between 0.1 and 18 μ s using Eq. (5).

in the μ^\pm beam. Since the decay asymmetry is very small and the lifetime of the μ^- depends upon the nucleus on which it captures, the histogram of μ^- SR was fitted by a combination of five different lifetimes τ_i :

$$N(t) = \sum_{i=1}^{n=5} N_i e^{-t/\tau_i} [1 + A_i e^{-\lambda_i t} \cos(\omega_i t + \phi_i)], \quad (1)$$

where N_i is a normalization constant at $t = 0$ for the i th muon lifetime (τ_i), A_i is the muon decay asymmetry for that process, ω_i is the angular frequency of the μ^- spin precession caused by the applied TF, and ϕ_i is the initial phase. As a first approximation, A_i is nonzero only for muonic oxygen (the main component) and negligible for the other elements, all of which have nuclear spins and therefore form hyperfine-coupled states with the μ^- , precessing at dramatically

different frequencies. Furthermore, since A_i is below 1/6 of A for μ^+ SR (typically 0.24) due to the reduction of spin polarization, $A_i < 0.04 (= 0.24/6) \ll 1$. Therefore, it is reasonable to fix $A_i = 0$ for the other minor elements to estimate each N_i using Eq. (1).

The fit showed that the first lifetime ($\tau_0 = 1.7954 \mu$ s) is predominant in the time domain between 0.5 and 10 μ s, where τ_0 means τ for μ^- captured on ¹⁶O [39]. The second, third, and fourth lifetimes represent muons captured on Li with $\tau_{\text{Li}} = 2.188 \mu$ s, ³¹P with $\tau_{\text{P}} = 0.6112 \mu$ s, and ⁵⁵Mn with $\tau_{\text{Mn}} = 0.2325 \mu$ s [39]. Since $\tau_5 [= 29.2(7) \mu$ s] is longer than τ for a free μ^\pm (2.19703 μ s), the fifth lifetime is caused by other particles, such as e^- , e^+ and/or neutrons, or other effects for reasons currently unknown. However, the contribution of the fifth lifetime is negligibly small for $t \lesssim 10 \mu$ s.

In contrast, the histogram of μ^+ SR includes only one component, i.e., $n = 1$ in Eq. (1), resulting in the linear relationship between $\log(N)$ and time together with the oscillation due to TF [Figs. 2(c) and 2(d)].

B. Asymmetry spectrum for μ^\pm SR

Figures 3(a) and 3(b) show the ZF- and LF- μ^- SR asymmetry spectra recorded at 100 and 300 K. Since the difference between ZF and LF spectra at 300 K is smaller than that at 100 K, we conclude that the internal magnetic field becomes dynamic with temperature. This is because LF = 50 Oe is enough large to decouple the nuclear magnetic field, which ranges typically below 10 Oe in solids. As a result, the LF spectrum shows an almost “nuclear-magnetic-field-free” behavior, particularly when the nuclear magnetic field is static. However, when the nuclear magnetic field becomes dynamic, such decoupling effect with LF is weakened depending on the fluctuation rate. Therefore, one can estimate the fluctuation rate from the ZF and LF spectra [40].

In the analysis of the μ^- SR asymmetry spectra, we disregard the small and short-lived contributions from μ^- P and μ^- Mn; the longer lived (but still small) contribution from μ^- Li, whose two hyperfine states [41] are both expected to be nonrelaxing, because muonic lithium acts like helium and diffuses freely through the Li metal lattice at room temperature, is included as a small nonrelaxing component.

As a result, each histogram is given by

$$N^{\text{F}}(t) = N_{\text{O}}^{\text{F}} \exp(-t/\tau_{\text{O}}) [1 - A_{\text{O}} G^{\text{DGKT}}(t, \Delta^-, \nu^-, H_{\text{LF}}) \exp(-\lambda_{\text{O}}^- t)] + N_{\text{Li}}^{\text{F}} \exp(-t/\tau_{\text{Li}}) (1 - A_{\text{Li}}), \quad (2)$$

$$N^{\text{B}}(t) = N_{\text{O}}^{\text{B}} \exp(-t/\tau_{\text{O}}) [1 + A_{\text{O}} G^{\text{DGKT}}(t, \Delta^-, \nu^-, H_{\text{LF}}) \exp(-\lambda_{\text{O}}^- t)] + N_{\text{Li}}^{\text{B}} \exp(-t/\tau_{\text{Li}}) (1 + A_{\text{Li}}). \quad (3)$$

Considering the fact that $N_{\text{O}} \gg N_{\text{Li}}$ and introducing the following three parameters, i.e., $\alpha_{\text{O}} \equiv N_{\text{O}}^{\text{B}}/N_{\text{O}}^{\text{F}}$, $\beta^{\text{F}} \equiv N_{\text{Li}}^{\text{F}}/N_{\text{O}}^{\text{F}}$, and $\beta^{\text{B}} \equiv N_{\text{Li}}^{\text{B}}/N_{\text{O}}^{\text{B}}$, the asymmetry spectrum is represented by

$$A_0 P(t) \sim \frac{N^{\text{B}} - \alpha_{\text{O}} N^{\text{F}}}{N^{\text{B}} + \alpha_{\text{O}} N^{\text{F}}} = \frac{A_{\text{O}} G^{\text{DGKT}}(t, \Delta^-, \nu^-, H_{\text{LF}}) \exp(-\lambda_{\text{O}}^- t) + \left[\frac{\beta^{\text{B}} - \beta^{\text{F}}}{2} + \frac{\beta^{\text{B}} + \beta^{\text{F}}}{2} A_{\text{Li}} \right] \exp\left(-\frac{t}{\tau_{\text{Li}}} + \frac{t}{\tau_{\text{O}}}\right)}{1 + \left[\frac{\beta^{\text{B}} + \beta^{\text{F}}}{2} + \frac{\beta^{\text{B}} - \beta^{\text{F}}}{2} A_{\text{Li}} \right] \exp\left(-\frac{t}{\tau_{\text{Li}}} + \frac{t}{\tau_{\text{O}}}\right)}, \quad (4)$$

where A_0 is the initial ($t = 0$) asymmetry, $P(t)$ is the muon spin polarization function, A_{O} and A_{Li} are the asymmetries associated with the signals from the μ^- captured on O and

Li, respectively, G^{DGKT} is a *dynamic* Gaussian Kubo-Toyabe function, Δ^- is the static width of the nuclear field distribution at the μ^- sites, ν^- is the fluctuation rate of the nuclear

fields, and λ_{O}^- is the exponential relaxation rate caused by localized $3d$ moments of Mn^{2+} ($3d^5$). Δ [ν] corresponds to a spin-spin relaxation rate ($1/T_2$) [a spin-lattice relaxation rate ($1/T_1$)] [8,9]. For $\nu = 0$ and $H_{\text{LF}} = 0$ (i.e., ZF), $G^{\text{DGKT}}(t, \Delta, \nu, H_{\text{LF}})$ becomes a *static* Gaussian Kubo-Toyabe function [42], $G_{zz}^{\text{KT}}(t, \Delta) = \frac{1}{3} + \frac{2}{3}(1 - \Delta^2 t^2) \exp(-\frac{1}{2}\Delta^2 t^2)$, which represents the internal magnetic field formed by randomly oriented static nuclear dipoles with Gaussian distribution.

The three parameters, α_{O} , β^{F} , and β^{B} , are determined from the histogram fit with Eq. (1), and τ_{O} and τ_{Li} are already reported as mentioned above. Furthermore, since $A_{\text{Li}} \approx 0.003$ based on the past μ^- -SR work on Li [41] and $\beta^{\text{F}} \sim \beta^{\text{B}} < 0.1$, we disregard the second term in Eq. (4). As a first step, the ZF- and LF- μ^- -SR spectra recorded at 100 K were fitted using common Δ^- , ν^- , and λ_{O}^- in the time domain between 0.5 and 3 μs . Such simultaneous fit provided that $\Delta^- = 0.49(4) \mu\text{s}^{-1}$ [corresponding to 5.7(4) Oe], $\nu^- = 0.0(5) \mu\text{s}^{-1}$, and $\lambda_{\text{O}}^- = 0.42(5) \mu\text{s}^{-1}$ at 100 K. Since dipole field calculations with DIPELEC [43] predicts that $\Delta_{\text{calc}}^- = 0.320 \mu\text{s}^{-1}$ (3.76 Oe) at the O sites in LiMnPO_4 , the present experimental result is comparable to the predicted value. Therefore, the nuclear magnetic field is effectively static at 100 K.

As a second step, the ZF- and LF- μ^- -SR spectra recorded at 100, 200, and 300 K were ‘‘global-fitted’’ using Eq. (4) with common $A_{\text{O}} [= 0.0091(2)]$, $\Delta^- (= 0.49 \mu\text{s}^{-1})$, and $\lambda_{\text{O}}^- (= 0.42 \mu\text{s}^{-1})$. Additionally, a time-independent background signal has been added to Eq. (4) in order to fit the nonlinear background signal from the τ_5 component contributing to the early time domain. Figure 4(a) shows the temperature dependences of Δ^- and ν^- for LiMnPO_4 determined with μ^- -SR measurements. Although the error is rather large due to a small asymmetry, ν^- starts to increase with temperature monotonically above 100 K. This clearly demonstrates Li diffusion in LiMnPO_4 above 100 K. If we fix Δ^- at Δ_{calc}^- , the estimated ν^- , i.e., ν_{fix}^- , increases with temperature more remarkably than the case that Δ^- is a free parameter.

Now we move on the μ^+ -SR results. Figures 3(c) and 3(d) show the ZF- and two LF- μ^+ -SR asymmetry spectra for LiMnPO_4 recorded at 100 and 300 K. As in the case for LiFePO_4 [12,13], the μ^+ -SR spectrum exhibits a highly damped Kubo-Toyabe behavior even in a paramagnetic state due to the effects of localized $3d$ moments of Mn^{2+} ions at the interstitial μ^+ sites. The ZF and LF spectra were therefore fitted by a combination of an exponentially relaxing G^{DGKT} [44], an exponential relaxation function, and a time-independent background signal from the μ^+ s stopped in the sample holder [12,13]:

$$A_0 P(t) = A_{\text{KT}} G^{\text{DGKT}}(t, \Delta^+, \nu^+, H_{\text{LF}}) \exp(-\lambda_{\text{KT}}^+ t) + A_{\text{F}} \exp(-\lambda_{\text{F}}^+ t) + A_{\text{BG}}, \quad (5)$$

where A_{KT} , A_{F} , and A_{BG} are the asymmetries associated with the three signals. As is the case for μ^- -SR, the ZF- and LF- μ^+ -SR spectra were fitted using common Δ^+ and ν^+ at each temperature. However, we used temperature-independent $A_{\text{KT}} [= 0.0378(4)]$, $A_{\text{F}} [= 0.0173(4)]$, $A_{\text{BG}} [= 0.0250(3)]$, $\lambda_{\text{F}}^+ [= 1.59(6) \mu\text{s}^{-1}]$, and $\lambda_{\text{KT}}^+ [= 0.203(5) \mu\text{s}^{-1}]$ in the whole temperature range measured. Such simultaneous

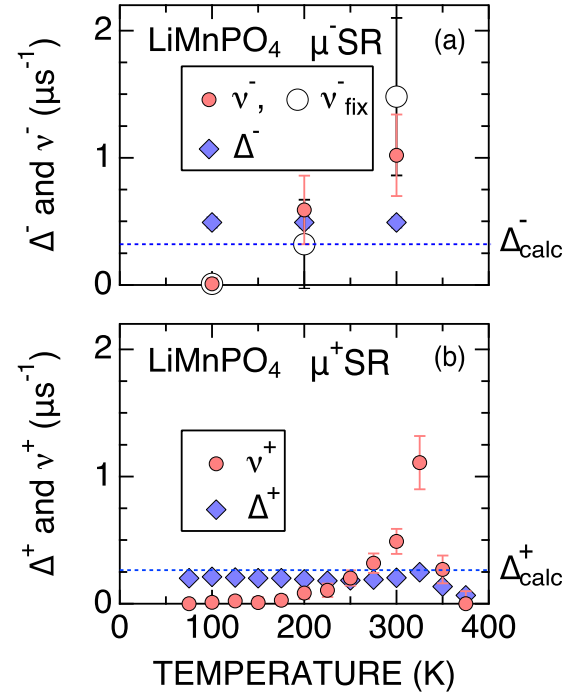


FIG. 4. The temperature dependences of Δ and ν for LiMnPO_4 determined with (a) μ^- -SR and (b) μ^+ -SR. The data were obtained by fitting the ZF- and LF- μ^\pm -SR spectra with Eqs. (4) and (5). In panel (a), ν_{fix}^- represents ν^- , when $\Delta^- = \Delta_{\text{calc}}^-$. The μ^+ sites predicted by DFT calculations with VASP were (0.135, 0.75, 0.587) and (0.195, 0.92, 0.89). A horizontal broken line shows the predicted Δ^\pm with dipole field calculations with DIPELEC [43].

fit for ZF- and LF- μ^+ -SR spectra in the time domain between 0.1 and 18 μs provided the temperature dependences of these parameters [Fig. 4(b)]. Both λ_{F}^+ and λ_{KT}^+ naturally come from the fluctuation of the localized Mn $3d$ moments [44]. According to the previous magnetization and μ^+ -SR measurements on LiMPO_4 with $M = \text{Fe, Co, and Ni}$ [13], λ_{F}^+ and λ_{KT}^+ are independent of temperature, while the magnetic susceptibility versus temperature curve exhibits a Curie-Weiss behavior above T_{N} (53, 25, and 23 K for $M = \text{Fe, Co, and Ni}$,

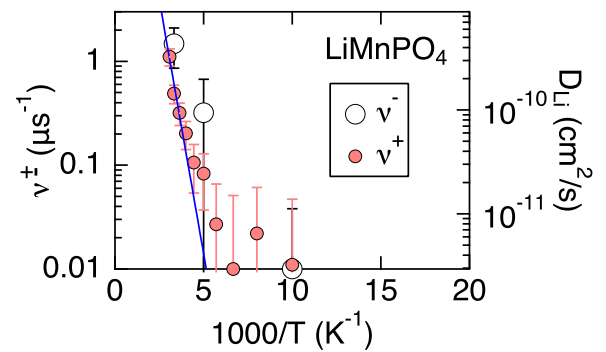


FIG. 5. The relationship between ν^\pm (D_{Li}) and inverse temperature. ν^\pm (D_{Li}) are estimated from the μ^\pm -SR results. ν^- for μ^- -SR is ν_{fix}^- in Fig. 4(a). Solid line represents the fit using a thermal activation process: $\nu = \nu_0 \exp(-E_a/k_B T)$ in the temperature range between 200 and 325 K, where E_a is the activation energy and k_B is Boltzmann’s constant.

respectively). This leads to the scenario in which the coupling constant between $3d$ moments and μ^+ spin in LiMPO₄ is rather small compared with temperature [13]. Therefore, we have applied a similar scenario to LiMnPO₄. This scenario was also used for the estimation of λ_{O}^- . Note that λ_{KT}^+ is comparable to λ_{O}^- from μ^- -SR [0.42(5) μs^{-1}], because the distance between μ^+ and Mn (2.24 and 2.26 Å) is close to that between μ^- , i.e., O and Mn (2.13–2.30 Å).

By comparing Figs. 4(a) and 4(b), we can see that the temperature dependence of v^- estimated with μ^- -SR is very similar to that of v^+ estimated with μ^+ -SR. Therefore, the fluctuations naturally originated from the same dynamic process. Since μ^- is immobile, the mobility of μ^+ itself must be irrelevant to the dynamic behavior. The dynamic process measured in both experiments is hence assigned as Li diffusion. Consequently, Li diffusion data can be obtained with μ^+ -SR, which is easier and provides better data than μ^- -SR. The decrease in v^+ above 325 K in Fig. 4(b) is most likely caused by the difficulty in the fit for the data with $v^+ \gg \Delta^+$. This is because the ZF- and LF- μ^+ -SR spectra under such condition exhibit an exponential relaxation behavior [see Fig. 3(d)], and, as a result, Eq. (5) is no longer suitable for analyzing the μ^+ -SR spectrum.

It should be noted that, in the above fitting procedure, the number of the temperature-dependent free parameters is reduced as small as possible and finally there is only one for μ^- -SR and two for μ^+ -SR, namely, v^- in Eq. (4) and Δ^+ and v^+ in Eq. (5) to avoid ambiguity of fitting.

IV. DISCUSSION

A. μ^- captured on O

In the μ^- -SR experiment, we have focused on the signal from the μ^- captured on O. The resulting muonic oxygen (μ^- -O) behaves as a nitrogen-like atom in the lattice, although the effect of μ^- -O on Li diffusion is still not clarified. In the LiMnPO₄ lattice (Fig. 1), each oxygen is bound to both P⁵⁺ and Mn²⁺. Therefore, the displacement of μ^- -O from the regular O position is restricted by two different cations. In fact, the estimated Δ^- is comparable to Δ_{calc}^- predicted for the regular O site [Fig. 4(a)], suggesting that the local distortion around μ^- -O is unlikely drastic.

The local charge distribution around μ^- -O is also altered by an additional negative charge brought by μ^- . This could suppress Li diffusion, while the experimental result shows that $v^- \sim v^+$ in the whole temperature range measured (Fig. 4). This is probably because Li diffusion is a thermally activated process over the whole lattice. As a result, μ^- -O detects the average fluctuation rate of the nuclear dipole field, even when the diffusive motion of the nearest neighboring Li is affected by μ^- -O.

B. Diffusion coefficient of Li⁺

Finally, we attempt to evaluate a self-diffusion coefficient of Li⁺ ions (D_{Li}) using the present μ^\pm -SR result. Since the regular Li site is fully occupied by Li, the observed v naturally corresponds to Li jump from a regular site to interstitial sites. Then, D_{Li} is given by [45]

$$D_{\text{Li}} = \sum_{i=1}^n \frac{1}{N_i} Z_{v,i} s_i^2 v, \quad (6)$$

where N_i is the number of Li sites in the i th path, $Z_{v,i}$ is the vacancy fraction, and s_i is the jump distance. Based on a similar discussion for LiFePO₄ [12,13,20,21], $n = 2$, $N_1 = 2$, and $Z_1 = 1$, $N_2 = 2$, and $Z_2 = 1$, $s_1 = 1.74$ Å and $s_2 = 1.69$ Å. Figure 5 shows the relationship between v^\pm (D_{Li}) and inverse temperature. The magnitude of D_{Li} at 300 K and the activation energy for Li diffusion are estimated $1.4(3) \times 10^{-10}$ cm²/s and 0.19(3) eV, respectively, and they are comparable to those for LiMPO₄ with $M = \text{Fe, Co, and Ni}$ [13].

V. SUMMARY

In summary, we have observed a diffusive behavior in the battery material LiMnPO₄ by both μ^+ -SR and μ^- -SR. This demonstrated that Li is more mobile than μ^+ in the olivine lattice, and, as a result, μ^\pm -SR provides essential information on Li diffusion in olivine-type compounds, even when they include magnetic ions. μ^\pm -SR is also available for other types of energy materials, in which ion diffusion plays a significant role for their function, such as, Na- and K-ion battery materials, fuel cell materials, hydrogen storage materials, photovoltaic materials, and so on.

ACKNOWLEDGMENTS

We thank the staff of ISIS and I. Umegaki of Toyota CRDL for help with the μ^\pm -SR experiments (RB1970006 [46] and RB1510265 [47]) and H. Lee of KEK for DFT calculations. M.M., Y.S., and O.K.F. were partly supported by the Swedish Research Council (VR) through a neutron project grant (BIFROST, No. 2016-06955). Y.S. also receive additional funding via a VR starting grant (No. 2017-05078). E.N. is fully financed by the Swedish Foundation for Strategic Research (SSF) within the Swedish national graduate school in neutron scattering (SwedNess). K.P. is financed by Chalmers Area of Advance-Materials Science. This work was supported by Japan Society for the Promotion Science (JSPS) KAKENHI Grant No. JP18H01863.

- [1] C. V. Chandran and P. Heitjans, *Solid-State NMR Studies of Lithium Ion Dynamics Across Materials Classes*, Annual Reports on NMR Spectroscopy Vol. 89 (Academic Press, New York, 2016), Chap. 1, pp. 1–102.
 [2] C. P. Grey and N. Dupré, *Chem. Rev.* **104**, 4493 (2004).

- [3] S. Trasatti and O. A. Petrii, *Pure Appl. Chem.* **63**, 711 (1991).
 [4] J. Sugiyama, K. Mukai, M. Harada, H. Nozaki, K. Miwa, T. Shiotsuki, Y. Shindo, S. R. Giblin, and J. Lord, *Phys. Chem. Chem. Phys.* **15**, 10402 (2013).
 [5] J. Sugiyama, *J. Phys. Soc. Jpn.* **85**, 091012 (2016).

- [6] D. Parfitt, A. Kordatos, P. P. Filippatos, and A. Chroneos, *Appl. Phys. Rev.* **4**, 031305 (2017).
- [7] J. Sugiyama, K. Mukai, Y. Ikedo, H. Nozaki, M. Månsson, and I. Watanabe, *Phys. Rev. Lett.* **103**, 147601 (2009).
- [8] G. M. Kalvius, D. R. Noakes, and O. Hartmann, *Handbook on the Physics and Chemistry of Rare Earths* (North-Holland, Amsterdam, 2001), Vol. 32, Chap. 206, pp. 55–451.
- [9] A. Yaouanc and P. D. de Reotier, *Muon Spin Rotation, Relaxation, and Resonance, Application to Condensed Matter* (Oxford, New York, 2011).
- [10] A. V. der Ven and G. Ceder, *Electrochem. Solid State Lett.* **3**, 301 (2000).
- [11] J. Sugiyama, Y. Ikedo, K. Mukai, H. Nozaki, M. Månsson, O. Ofer, M. Harada, K. Kamazawa, Y. Miyake, J. H. Brewer *et al.*, *Phys. Rev. B* **82**, 224412 (2010).
- [12] J. Sugiyama, H. Nozaki, M. Harada, K. Kamazawa, O. Ofer, M. Månsson, J. H. Brewer, E. J. Ansaldo, K. H. Chow, Y. Ikedo *et al.*, *Phys. Rev. B* **84**, 054430 (2011).
- [13] J. Sugiyama, H. Nozaki, M. Harada, K. Kamazawa, Y. Ikedo, Y. Miyake, O. Ofer, M. Månsson, E. J. Ansaldo, K. H. Chow *et al.*, *Phys. Rev. B* **85**, 054111 (2012).
- [14] J. Sugiyama, K. Mukai, H. Nozaki, M. Harada, M. Månsson, K. Kamazawa, D. Andreica, A. Amato, and A. D. Hillier, *Phys. Rev. B* **87**, 024409 (2013).
- [15] J. Sugiyama, H. Nozaki, I. Umegaki, K. Mukai, K. Miwa, S. Shiraki, T. Hitosugi, A. Suter, T. Prokscha, Z. Salman *et al.*, *Phys. Rev. B* **92**, 014417 (2015).
- [16] J. Sugiyama, I. Umegaki, T. Uyama, R. M. L. McFadden, S. Shiraki, T. Hitosugi, Z. Salman, H. Saadaoui, G. D. Morris, W. A. MacFarlane *et al.*, *Phys. Rev. B* **96**, 094402 (2017).
- [17] I. Umegaki, S. Kawauchi, H. Sawada, H. Nozaki, Y. Higuchi, K. Miwa, Y. Kondo, M. Månsson, M. Telling, F. C. Coomer *et al.*, *Phys. Chem. Chem. Phys.* **19**, 19058 (2017).
- [18] A. S. Powell, J. S. Lord, D. H. Gregory, and J. J. Titman, *J. Phys. Chem. C* **113**, 20758 (2009).
- [19] A. S. Powell, Z. Stoeva, J. S. Lord, R. I. Smith, D. H. Gregory, and J. J. Titman, *Phys. Chem. Chem. Phys.* **15**, 816 (2013).
- [20] P. J. Baker, I. Franke, F. L. Pratt, T. Lancaster, D. Prabhakaran, W. Hayes, and S. J. Blundell, *Phys. Rev. B* **84**, 174403 (2011).
- [21] T. E. Ashton, J. V. Laveda, D. A. MacLaren, P. J. Baker, A. Porch, M. O. Jones, and S. A. Corr, *J. Mater. Chem. A* **2**, 6238 (2014).
- [22] I. D. Johnson, T. E. Ashton, E. Blagovidova, G. J. Smales, M. Lübke, P. J. Baker, S. A. Corr, and J. A. Darr, *Sci. Rep.* **8**, 4114 (2018).
- [23] M. Medarde, M. Mena, J. L. Gavilano, E. Pomjakushina, J. Sugiyama, K. Kamazawa, V. Y. Pomjakushin, D. Sheptyakov, B. Batlogg, H. R. Ott *et al.*, *Phys. Rev. Lett.* **110**, 266401 (2013).
- [24] M. Månsson and J. Sugiyama, *Phys. Scr.* **88**, 068509 (2013).
- [25] J. Sugiyama, H. Nozaki, I. Umegaki, M. Harada, Y. Higuchi, E. J. Ansaldo, J. H. Brewer, Y. Miyake, G. Kobayashi, and R. Kanno, *J. Phys.: Conf. Ser.* **551**, 012012 (2014).
- [26] I. Umegaki, H. Nozaki, M. Harada, M. Månsson, H. Sakurai, I. Kawasaki, I. Watanabe, and J. Sugiyama, *JPS Conf. Proc.* **21**, 011018 (2018).
- [27] J. Sugiyama, I. Umegaki, H. Nozaki, W. Higemoto, K. Hamada, S. Takeshita, A. Koda, K. Shimomura, K. Ninomiya, and M. K. Kubo, *Phys. Rev. Lett.* **121**, 087202 (2018).
- [28] K. M. Kojima, T. Murakami, Y. Takahashi, H. Lee, S. Y. Suzuki, A. Koda, I. Yamauchi, M. Miyazaki, M. Hiraishi, H. Okabe *et al.*, *J. Phys.: Conf. Ser.* **551**, 012063 (2014).
- [29] S. Devons and I. Duerdoth, *Muonic Atoms*, Advances in Nuclear Physics (Springer, New York, 1969).
- [30] K. Momma and F. Izumi, *J. Appl. Crystallogr.* **41**, 653 (2008).
- [31] A. K. Padhi, K. S. Nanjundaswamy, and J. B. Goodenough, *J. Electrochem. Soc. India* **144**, 1188 (1997).
- [32] A. Yamada, Y. Takei, H. Koizumi, N. Sonoyama, R. Kanno, K. Itoh, M. Yonemura, and T. Kamiyama, *Chem. Mater.* **18**, 804 (2006).
- [33] B. L. Ellis, K. T. Lee, and L. F. Nazar, *Chem. Mater.* **22**, 691 (2010).
- [34] M. Köntje, M. Memm, P. Axmann, and M. Wohlfahrt-Mehrens, *Prog. Solid State Chem.* **42**, 106 (2014).
- [35] S.-i. Nishimura, G. Kobayashi, K. Ohoyama, R. Kanno, M. Yashima, and A. Yamada, *Nat. Mater.* **7**, 707 (2008).
- [36] S. B. Sulaiman, S. Srinivas, N. Sahoo, F. Hagelberg, T. P. Das, E. Torikai, and K. Nagamine, *Phys. Rev. B* **49**, 9879 (1994).
- [37] J. Sugiyama, J. H. Brewer, E. J. Ansaldo, H. Itahara, K. Dohmae, Y. Seno, C. Xia, and T. Tani, *Phys. Rev. B* **68**, 134423 (2003).
- [38] A. Suter and B. Wojek, *Phys. Proc.* **30**, 69 (2012).
- [39] T. Suzuki, D. F. Measday, and J. P. Roalson, *Phys. Rev. C* **35**, 2212 (1987).
- [40] R. S. Hayano, Y. J. Uemura, J. Imazato, N. Nishida, T. Yamazaki, and R. Kubo, *Phys. Rev. B* **20**, 850 (1979).
- [41] D. Favart, F. Brouillard, L. Grenacs, P. Igo-Kemenes, P. Lipnik, and P. C. Macq, *Phys. Rev. Lett.* **25**, 1348 (1970).
- [42] R. Kubo and T. Toyabe, *Magnetic Resonance and Relaxation* (North-Holland, Amsterdam, 1996).
- [43] K. M. Kojima, J. Yamanobe, H. Eisaki, S. Uchida, Y. Fudamoto, I. M. Gat, M. I. Larkin, A. Savici, Y. J. Uemura, P. P. Kyriakou *et al.*, *Phys. Rev. B* **70**, 094402 (2004).
- [44] T. Matsuzaki, K. Nishiyama, K. Nagamine, T. Yamazaki, M. Senba, J. M. Bailey, and J. H. Brewer, *Phys. Lett. A* **123**, 91 (1989).
- [45] R. J. Borg and G. J. Dienes, *An Introduction to Solid State Diffusion* (Academic Press, San Diego, 1988), Chap. 3, pp. 53–77.
- [46] J. Sugiyama, Determination of diffusing species in LiFePO₄ with negative muons, STFC ISIS facility, RIKEN-RAL Muon facility, 2019, <https://doi.org/10.5286/ISIS.E.RB1970006>.
- [47] J. Sugiyama, Li diffusion in complex olivine, Li(FeMn)PO₄, STFC ISIS facility, 2015, <https://doi.org/10.5286/ISIS.E.RB1510265>.